

# Theoretical Analysis of Bandwidth Requirements for Damped Sinusoid Measurement

Jing Yang<sup>1,2,\*</sup>, Wei Wu<sup>2</sup>, Zhizhen Zhu<sup>2</sup>, Zhitong Cui<sup>2</sup>, Yayun Dong<sup>2</sup>,  
Xin Nie<sup>2</sup>, Fei Cao<sup>1</sup>, and Chuan He<sup>1</sup>

<sup>1</sup>*Xi'an Research Institute of High Technology, Xi'an, China*

<sup>2</sup>*Northwest Institute of Nuclear Technology, Xi'an, China*

**ABSTRACT:** High altitude electromagnetic pulse (HEMP) couples to cables and introduces interference into the connected electronic equipment. Responses arising from the transient electromagnetic field typically follow an exponentially damped sinusoid behavior. Thus, damped sinusoids with different parameters are recommended in the International Electrotechnical Commission (IEC) standards as typical injected waveforms for HEMP conducted immunity test. To guarantee the compliance of the injected pulse, accurate measurement of the injected pulse is needed. Wideband proportional current sensors are often applied to measure the injected damped sinusoid. However, bandwidth requirements of wideband proportional current sensor for damped sinusoid measurement are not specified. In this paper, two formulae are deduced to establish the relationships between the bandwidth requirements and the fundamental resonance frequency of the damped sinusoid to be measured. It is convenient and simple for the on-site engineers to check whether the bandwidth of the proportional current sensor is suitable by the formulae. Monte-Carlo simulation is conducted in support of the recommended formulae.

## 1. INTRODUCTION

High-altitude electromagnetic pulse (HEMP) [1] introduces interference current into the electronic equipment. Antennas and the interconnected cables are the main coupling paths. Most coupling currents at the port of entry of the equipment follow an exponentially damped sinusoidal behavior. International Electrotechnical Commission (IEC) standard, IEC 61000-2-10, describes the response of a dipole antenna excited by the early-time HEMP as damped sinusoidal pulse [2]. Thus, exponentially damped sinusoids are recommended as the waveforms for HEMP conducted immunity tests by IEC 61000-4-25 [3] and MIL-STD 461F [4] (CS116). It is important to measure the injected damped sinusoidal pulse accurately to guarantee the compliance of the HEMP conducted immunity test to the standards.

Wideband current sensors are often applied to measure the damped sinusoidal pulse. Based on the response mechanism, the wideband sensors can be divided into proportional ones and derivation ones. Proportional ones are commonly used for transient pulse measurement. Because for proportional sensors, the signal to be measured can be rebuilt simply by multiplying the output by a constant. The constant is the reciprocal of sensitivity of the sensor. The sensitivity can be obtained either by referring to the specification of the proportional current sensor (e.g., the sensitivity of a commercial proportional current sensor PEARSON CURRENT MONITOR MODEL 8585C is 1 V/A [8]) or by laboratory calibration.

The bandwidth of a sensor has critical impact on the accuracy of the measured result rebuilt by its sensitivity. Thus, it is an important parameter for the selection of a proper proportional current sensor. The bandwidth is defined as a frequency range over  $f_{\min}$  to  $f_{\max}$ , where  $f_{\min}$  and  $f_{\max}$  are the low and high  $-3$  dB cutoff frequencies of the sensor, respectively, and the frequency response of the proportional current sensor should be flat.  $f_{\min}$  and  $f_{\max}$  are also provided in the specifications of the proportional current sensors (e.g., the  $f_{\min}$  to  $f_{\max}$  of a commercial proportional current sensor PEARSON CURRENT MONITOR MODEL 8585C are 1500 Hz to 200 MHz respectively [8]).  $f_{\min}$  and  $f_{\max}$  can also be estimated by the impulse response of the sensors [7]. It needs to mention that only the bandwidth requirement is discussed in this paper. In fact, dynamic range, physical dimensions of the current sensor, and other parameters should be taken into consideration for the selection of a proper current sensor.

Empirical formula or estimation method of bandwidth requirements for another two kinds of typical injected pulse (i.e., the rectangular/trapezoidal pulse and double exponential pulse) measurement already exists. However, currently there are no related reports about the bandwidth requirements for damped sinusoid measurement. Concretely, empirical formula  $f_{\max} = 0.35/(\text{pulse rise time})$  is often applied as the bandwidth requirement of proportional sensors for rectangular pulse measurement. For some commercial current sensors, 'Usable rise time' and 'droop' are parameters provided in the specifications for rectangular pulse measurement [8]. As for double exponential pulse measurement, bandwidth requirements are discussed in [5]. IEC 61000-4-25 [3] also provides the required frequency

\* Corresponding author: Jing Yang (18392961969@163.com).

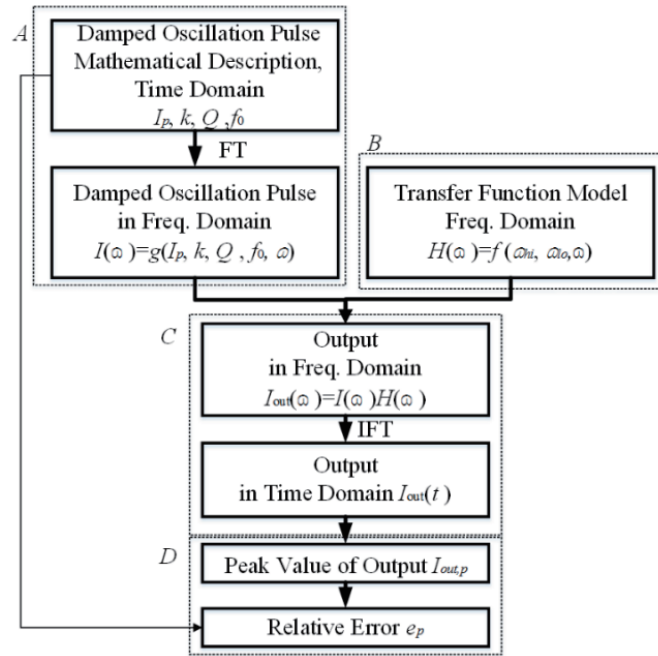


FIGURE 1. Overview of the simulation. Symbols *A*, *B*, *C*, *D* indicates the relevant sub-sections.

range of the overall measurement system for double exponential pulse measurement. However, as a commonly used injected pulse, bandwidth requirements of the current sensors for damped sinusoid have not been specified yet. In general, when damped sinusoid is measured, the bandwidth of the pulse current sensor should cover the resonance frequency first and as wide as possible. Quantitative analysis is needed.

In this paper, the bandwidth requirements of the proportional current sensor for damped sinusoid measurement are analyzed theoretically. The measurement procedure is modeled as an ideal damped oscillation pulse passing through a wideband current sensor. The frequency response of the wideband current sensor is modeled as the cascade of an ideal low-pass filter and an ideal high-pass filter [5, 6] based on its frequency response characteristic. The output of the model is then deduced theoretically. The peak value relative error of the rebuilt pulse and the original input is calculated as a parameter to evaluate the influence of the bandwidth. Without loss of generality, the input is normalized, and the sensitivity of the proportional current sensor is set as 1 V/A. Relationships between the relative error of the peak value and the bandwidth of the proportional current sensor are analyzed. Two simple formulae are summarized for the bandwidth requirements estimation. Then, the bandwidth requirements can be calculated directly according to the fundamental resonance frequency of the signal to be measured. Monte-Carlo simulation is done in support of the conclusion.

This paper is organized as follows. Section 2 introduces the models of input, pulse current sensor, and output. Section 3 provides the theoretical analysis results. Section 4 provides the Monte-Carlo simulation results in support of the theoretical analysis result and shows how to use the deduced formulae. The last section summarizes the whole paper.

## 2. MODEL OF MEASUREMENT

The measurement procedure is modelled as an ideal damped oscillation pulse passing through a band-pass filter theoretically. The block diagram of the procedure is shown in Fig. 1. The simulation is designed to obtain the relative error of the peak value based on the mathematical description of damped sinusoid and the transfer function model of the wideband current sensor. Subsections 2.1 and 2.2 introduce the mathematical description of damped sinusoid and the general transfer function model of wideband current sensor. Subsection 2.3 derives the output in frequency domain and then transforms it to time domain by inverse Fourier transformation to obtain the peak value of the output pulse. Post data processing procedure is introduced in Subsection 2.4. Relative error of the peak value is calculated to assess the effect of the limited bandwidth.

### 2.1. Mathematical Description of Damped Sinusoid

The damped sinusoids can be described by three scalar parameters including peak value, damping parameter  $Q$ , and fundamental resonance frequency  $f_0$ .

The exponentially damped sinusoid is expressed as (1) [2],

$$I(t) = kI_p e^{-\frac{\omega_0 t}{2Q}} \sin(\omega_0 t) u(t) \quad (1)$$

where  $\omega_0 = 2\pi f_0$ ,  $k$  is a normalizing factor,  $I_p$  the peak value of the damped sinusoid, and  $u(t)$  the Heaviside unit step function. The waveform of a typical damped sinusoid with  $Q = 10$  and  $f_0 = 50$  MHz is illustrated in Fig. 2 as an example. The damped sinusoid is the product of three terms, i.e., exponential decay term, sine term, and unit step function. The larger the  $Q$  is, the closer the first few cycles of the waveform are to the corresponding sine wave. Resonance quality factor  $Q$  represents

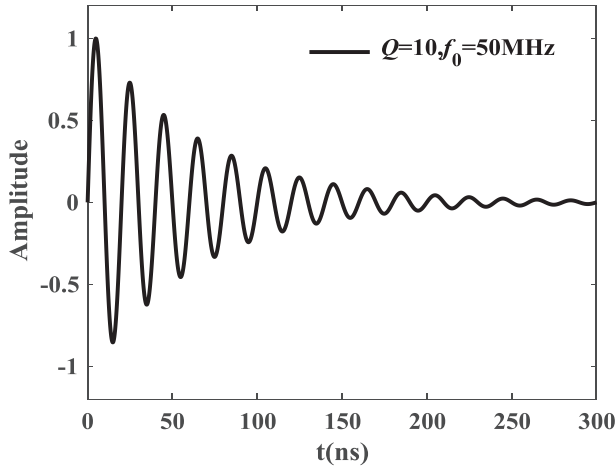


**FIGURE 2.** Waveform of a typical damped sinusoid.  $Q = 10$  and  $f_0 = 50$  MHz as an example. The amplitude is normalized.

the damping rate of the oscillatory wave, and its typical value is between 10 and 20.

The  $Q$  specified in [3] and [4] for HEMP conducted community test ranges from 6 to 33. The resonance frequencies of the injected current for HEMP conducted immunity test are also specified in [3] and [4]. For HEMP coupling current,  $Q$  and  $f_0$  are both closely related to the geometry of the wire bundle/antenna, incident field, and environment (parameters of the ground, air, other conducting bodies, etc.) It is difficult to take into account all the possibilities. In practice,  $Q$  and  $f$  are often estimated by the length of the line [2]. For a dipole antenna,  $f$  and  $Q$  can be calculated by (2) and (3)

$$f_0 = c/2l \quad (2)$$

$$Q = 2 \ln(l/a) / 3.6 \quad (3)$$

where  $l$  and  $a$  are the length and radius of the wire or antenna irradiated by HEMP, respectively.  $c$  is the speed of light in free space. Furthermore, without losing generality,  $I_p$  is set as 1 for the simplification of the derivation process in this paper.

The frequency spectrum of the damped sinusoid can be derived by Fourier transformation as (4).

$$I(\omega) = \frac{kI_p\omega_0}{(\omega_0/2Q + j\omega)^2 + \omega_0^2} \quad (4)$$

The amplitude of  $I(\omega)$  can be derived as (5),

$$|I(\omega)| = \frac{kI_p\omega_0}{\sqrt{[\omega^2 - (\omega_0^2 - \omega_0^2/4Q^2)]^2 + \omega_0^4/Q^2}} \quad (5)$$

$|I(\omega)|$  reaches its maximal value at  $\omega'_0 = \omega_0\sqrt{1 - 1/4Q^2}$ . Correspondingly,

$$f'_0 = f_0\sqrt{1 - 1/4Q^2} \quad (6)$$

If  $Q$  changes from 2 to 50,  $f'_0$  changes from  $0.97f_0$  to  $f_0$  approximately. The results show that the spectrum is wider, and the peak frequency shifts slightly compared with sine waves.

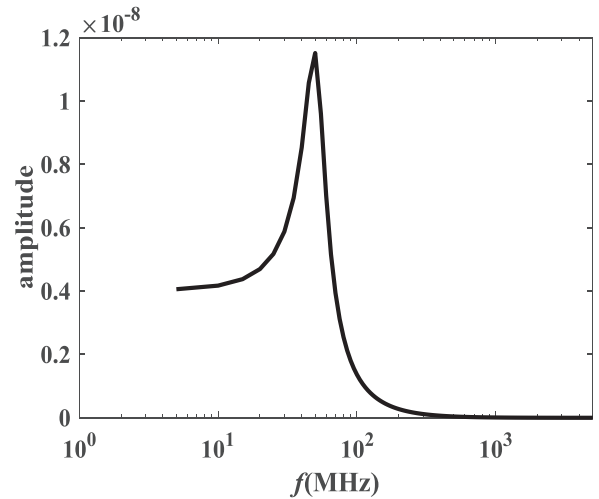


**FIGURE 3.** Amplitude spectrum of the damped sinusoid illustrated in Fig. 2. ( $Q = 10$  and  $f_0 = 50$  MHz).

The amplitude spectrum is illustrated in Fig. 3 ( $Q = 10$  and  $f_0 = 50$  MHz is set as an example).

When measuring a damped sinusoidal pulse, the bandwidth of the pulse current sensor should cover  $f'_0$  first, and the bandwidth should be as wide as possible to recover the exponential term correctly. Quantitative analysis is provided in the following discussion based on the band-pass filter model of the wideband current sensor.

## 2.2. Frequency Response Model of the Current Sensor

$-3$  dB bandwidth is the main characteristic of the current sensor that influences the output. For a proportional current sensor, the magnitude-frequency response is flat within the  $-3$  dB bandwidth. The  $-3$  dB bandwidth is typically provided in the specification or product manual. The bandwidth is defined as a frequency range over  $f_{\min}$  to  $f_{\max}$ . Thus, the frequency response of the wideband current sensor is modeled as an ideal low-pass and an ideal high-pass filters. The model is built and experimentally verified [5]. According to [5], the transfer functions of these two ideal filters can be expressed as (7) and (8) respectively.

$$H_{LP}(\omega) = \frac{\omega_{hi}}{j\omega + \omega_{hi}} \quad (7)$$

$$H_{HP}(\omega) = \frac{j\omega}{j\omega + \omega_{lo}} \quad (8)$$

where  $\omega_{hi} = 2\pi f_{\max}$  and  $\omega_{lo} = 2\pi f_{\min}$ .

Thus, the frequency response of the wideband current sensor can be expressed as (9).

$$H(\omega) = H_{LP}(\omega) H_{HP}(\omega) \quad (9)$$

To simplify the analysis, we set

$$\omega_{hi} = p \cdot \omega_0 \quad (10)$$

and

$$\omega_{lo} = q \cdot \omega_0 \quad (11)$$

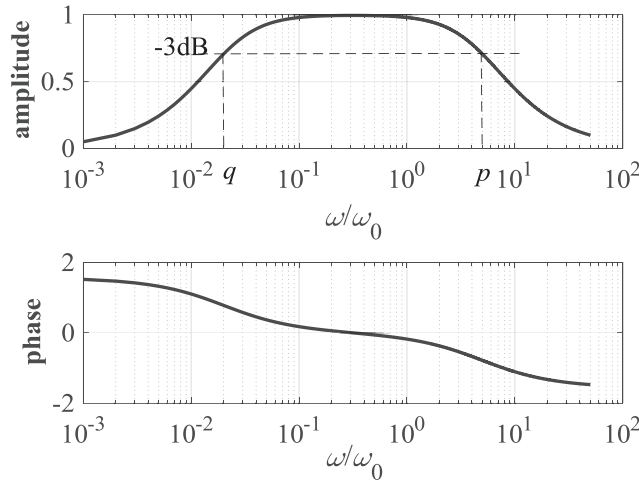


**FIGURE 4.** Amplitude spectrum and angle spectrum of the band-pass filter model for proportional current sensor.  $f_{\max}$  and  $f_{\min}$  equal  $0.02f_0$  and  $5f_0$  respectively as an example ( $q = 0.02$ ,  $p = 5$ ).

where  $p > 1$  and  $0 < q < 1$  to keep the fidelity of the output of the proportional sensor. Parameters  $p$  and  $q$  can be regarded as the relative angular frequencies.

The frequency response of the bandpass filter model is shown in Fig. 4.  $f_{\max}$  and  $f_{\min}$  equal  $0.02f_0$  and  $5f_0$  respectively as an example ( $q = 0.02$ ,  $p = 5$ ). When  $\omega = \omega_0$ , the absolute value of  $H(\omega)$  equals 0.98 for the example.

### 2.3. Output

The output of the frequency response model can be expressed as (12)[9].

$$I_{out}(\omega) = I(\omega) H(\omega) \quad (12)$$

The output in time domain can be derived by Fourier transformation (see Appendix A) as (13).

$$I_{out}(t) = kI_p \left[ \frac{A \exp(-\omega_{lo}t) + B \exp(-\omega_{hi}t) + \sqrt{C^2 + D^2} \exp\left(-\frac{\omega_0 t}{2Q}\right) \sin(\omega_0 t + \varphi)}{\sqrt{C^2 + D^2}} \right] u(t) \quad (13)$$

where

$$\begin{cases} A = -\frac{pq}{(1/2Q - q)^2 + 1} \frac{1}{p - q} \\ B = \frac{p^2}{(1/2Q - p)^2 + 1} \frac{1}{p - q} \\ C = -\frac{p(1/4Q^2 + 1 - pq)}{\left[ (1/2Q - p)^2 + 1 \right] \left[ (1/2Q - q)^2 + 1 \right]} \\ D = \frac{p(1/4Q^2 + 1)(p - 1/2Q + q) - p^2q/2Q}{\left[ (1/2Q - p)^2 + 1 \right] \left[ (1/2Q - q)^2 + 1 \right]} \end{cases}$$

and  $\varphi = \arctan(C/D)$ .

The output is shifted by a fixed angle. The degree of deviation depends on  $\varphi/\omega_0 t$ .

### 2.4. Post Processing

Relative error of the peak value is a critical parameter to evaluate the distortion from the input. Percentage relative error of the peak value  $e_p$  is defined as (14).

$$e_p = \frac{I_{out,p} - I_p}{I_p} \times 100\% \quad (14)$$

where  $I_p$  and  $I_{out,p}$  are the peak values of  $I$  and  $I_{out}$ , respectively.

## 3. THEORETICAL ANALYSIS

The expression for the output is complex and difficult to analyze. However, as  $\omega_{hi} \gg \omega_{lo}$  for most wideband proportional current sensors, the influence of  $f_{\max}$  and  $f_{\min}$  can be analyzed respectively.

### 3.1. Relative Error of the Peak Value Versus $f_{\max}$

Thus, we first set  $\omega_{lo} = 0$ . Then, the peak value of output is directly influenced by  $\omega_{hi}$ . The output of proportional current sensor can be derived as (15) by a similar method shown in Appendix A.

$$I_{out}(t)|_{q=0} = kI_p \left[ \frac{\kappa_1 \exp(-\omega_{hi}t) + \kappa_2 \exp(-\omega_0 t/2Q) \sin(\omega_0 t + \varphi)}{\kappa_1 + \kappa_2} \right] u(t) \quad (15)$$

where

$$\begin{cases} \kappa_1 = \frac{p}{(p - 1/2Q)^2 + 1} \\ \kappa_2 = \frac{p}{\sqrt{(p - 1/2Q)^2 + 1}} \end{cases}$$

and

$$\varphi|_{q=0} = -\arctan\left(\frac{1}{p - 1/2Q}\right).$$

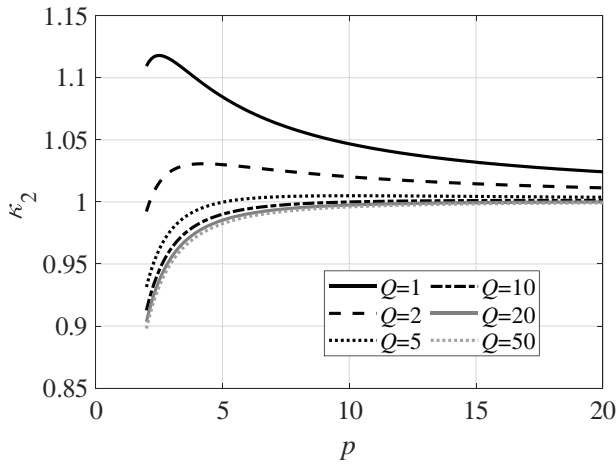


**FIGURE 5.** Coefficients of output  $\kappa_2$  versus  $p$  (relative  $f_{\max}$  of the proportional current sensor) for several typical  $Q$ . The curves are plotted based on the assumption that  $f_{\min} = 0$ , i.e.,  $p = 0$ .

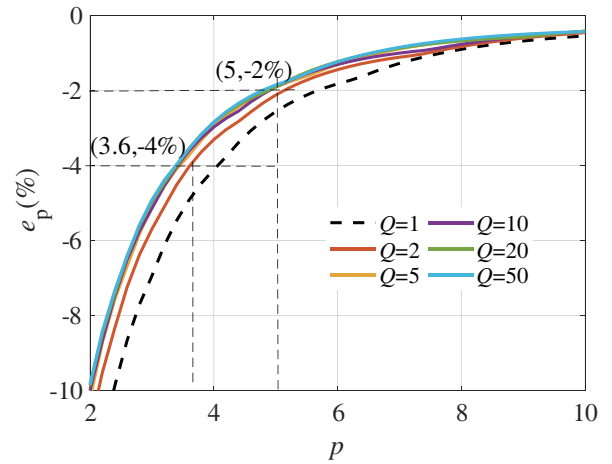


**FIGURE 6.** Relative error of the peak value  $e_p$  versus  $p$  for several typical  $Q$ . Two typical points are marked as a reference. The curves are plotted based on the assumption that  $f_{\min} = 0$ , i.e.,  $p = 0$ .

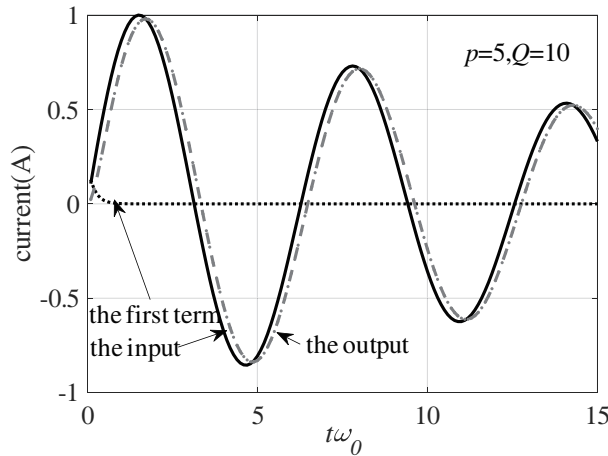


**FIGURE 7.** Output of the model ( $p = 5$ ,  $q = 0$ ,  $Q = 10$  as an example). Input (solid line) and the newly-emerged exponential decay term (dotted line) are also plotted as a reference. Only the first few cycles are shown in the figure. And the time-axis is the product of time and the angular frequency.

Equation (15) indicates that a new exponential decay term emerges (the first term of (15)). As  $\kappa_1 > 0$ , the first term is a positive number. When  $\omega_{hi} \gg \omega/2Q$ , i.e.,  $p \gg 1/2Q$ , the first term of (15) declines much faster than the second term, and the effect of the first term on the peak value can be ignored. The coefficient of output  $\kappa_2$  versus  $p$  for several typical  $Q$  is shown in Fig. 5. When  $p \gg 1/2Q$ , we need  $p^2 \gg 1$  to make the coefficient of the second term of (15) (i.e.,  $\kappa_2$ ) approaches 1. Relative error of the peak value  $e_p$  versus  $p$  for several typical  $Q$  is shown in Fig. 6. The curves are almost overlapped for  $Q > 2$ . The relative error of the peak value is  $-2\%$  approximately when  $q > 5$  (and  $-4\%$  when  $q > 3.6$ ) for  $Q > 2$  according to the curves shown in Fig. 6.

Output of the model when  $p = 5$ ,  $q = 0$ ,  $Q = 10$  as an example is shown in Fig. 7. Input (solid line) and the newly-emerged exponential decay term (dotted line) are also plotted as a reference. As  $\varphi < 0$ , the output lags the input by a fixed angle. As  $p = 5$  for the given example, the relative error of the

peak value is less than  $2\%$ . The results are consistent with the analysis above.

### 3.2. Relative Error of the Peak Value Versus $f_{\min}$

Second, assuming that  $\omega_{hi}$  is infinite, i.e.,  $p \rightarrow +\infty$ , the peak value and waveform of output are directly influenced by  $\omega_{lo}$ . Then,  $I_{out}$  can be deduced as (16)

$$I_{out}(t)|_{p \rightarrow +\infty} = kI_p \left[ \chi_1 \exp(-\omega_{lo}t) + \chi_2 \exp\left(-\frac{\omega_{ot}}{2Q}\right) \sin(\omega_0 t + \varphi) \right] u(t) \quad (16)$$

where

$$\begin{cases} \chi_1 = \frac{-q}{1 + (1/2Q - q)^2} \\ \chi_2 = \frac{\sqrt{q^2 + (1 + 1/4Q^2 - q/2Q)^2}}{1 + (1/2Q - q)^2} \end{cases}$$

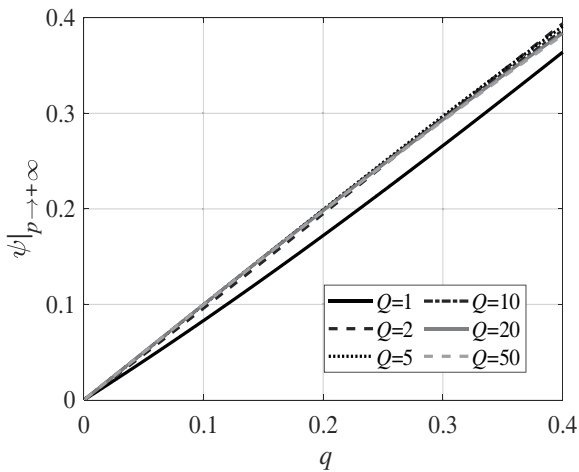


**FIGURE 8.** Shifting angle  $\varphi$  versus  $q$  (relative  $-3$  dB  $f_{\min}$  of the proportional current sensor) for six typical  $Q$ . The curves are plotted based on the assumption that  $f_{\max} \rightarrow +\infty$ , i.e.,  $q \rightarrow +\infty$ .

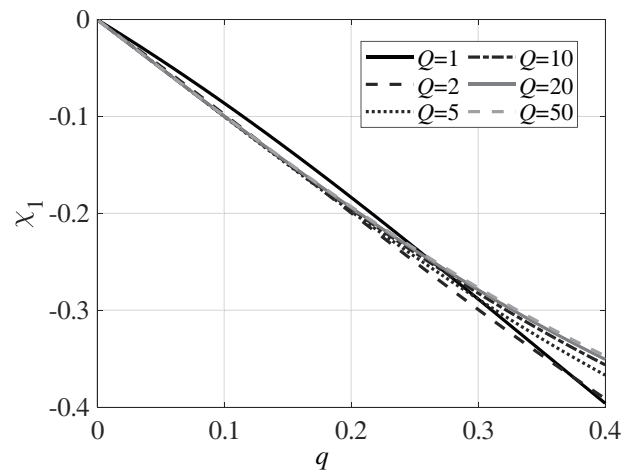


**FIGURE 9.** The value of the first term of the output  $\chi_1$  of versus  $q$  (relative  $-3$  dB  $f_{\min}$  of the proportional current sensor) for several typical  $Q$ . The curves are plotted based on the assumption that  $f_{\max} \rightarrow +\infty$ , i.e.,  $q \rightarrow +\infty$ .

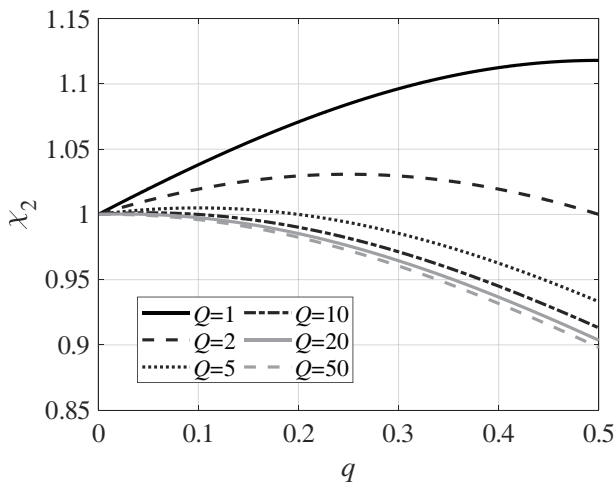


**FIGURE 10.** Coefficients of the output  $\chi_2$  of versus  $q$  for several typical  $Q$ . The curves are plotted based on the assumption that  $f_{\max} \rightarrow +\infty$ , i.e.,  $q \rightarrow +\infty$ .

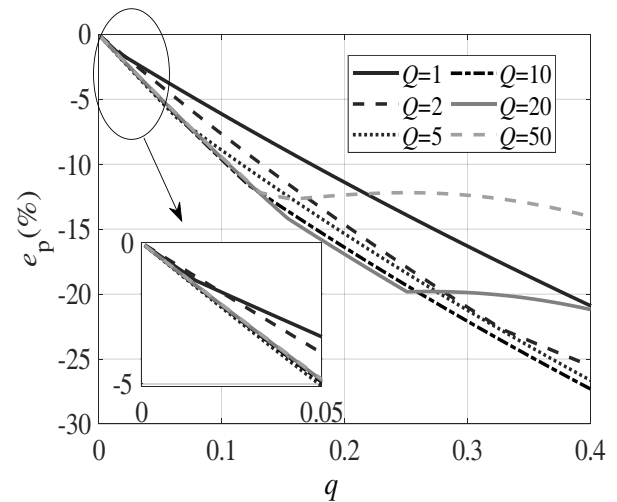


**FIGURE 11.** Relative error of the peak value  $e_p$  versus  $q$  for several typical  $Q$ . The initial part of the figure is locally zoomed up. The curves are plotted based on the assumption that  $f_{\max} \rightarrow +\infty$ , i.e.,  $q \rightarrow +\infty$ .

and

$$\varphi|_{p \rightarrow +\infty} = \arctan\left(\frac{q}{1 + 1/4Q^2 - q/2Q}\right)$$

When  $q$  is small enough,  $\chi_1 \rightarrow 0$ ,  $\chi_2 \rightarrow 1$ ,  $I_{out}(t)$  equals  $I(t)$  approximately. Equation (16) also indicates that a new exponential decay term emerges, and the peak value is  $\chi_2$  times the original. Meanwhile, the output is shifted by a fixed angle  $\varphi$ .

Curves of shifting angle  $\varphi$  versus  $q$  for six typical  $Q$  are shown in Fig. 8. The curves of  $\varphi$  overlap and are proportional to  $q$  (i.e.,  $\varphi \approx q$ ) for  $Q > 2$  when  $q$  is small. Thus, from the perspective of wave shifting, the smaller the  $q$  is, the better. The second term of (16) gets its maximal value when  $\omega_0 t \approx \pi/2 - q$ .

Coefficients of output ( $\chi_1$  and  $\chi_2$ ) versus  $q$  for several typical  $Q$  are shown in Fig. 9 and Fig. 10, respectively. The curves of  $\chi_1$  overlap and are proportional to  $q$  (i.e.,  $\chi_1 \approx -q$ ) approximately when  $q < 0.2$  for  $Q \geq 2$ . When  $Q$  equals 1 and 2, the

coefficient of the second term  $\chi_2$  has opposite sign to  $\chi_1$  and will compromise the impact of the first term to some extent on the initial stage. As  $\omega_{lo} < \omega_{hi}$ , the influence of the first term last longer than (15). The effect of the first term on the first few peaks cannot be ignored. Thus, the peak value of the output may be not the first peak but the following one.

Curves of relative error of the peak value  $e_p$  versus  $q$  for several typical  $Q$  are shown in Fig. 11. As only small  $e_p$  is of interest, the initial part of the figure is locally zoomed up at the bottom left corner of the figure. The curves of  $e_p$  overlap and are proportional to  $q$  (i.e.,  $e_p \approx -q$ ) roughly when  $q < 0.1$ . The curves of  $Q = 1$  and  $Q = 2$  seem to have better performance for small  $q$  from the perspective of relative error of peak value. This is because  $\chi_2 > 1$  for  $Q < 5$ , which partly offsets the effect of the first term on the peak value. Fig. 11 also shows that  $e_p$  does not decline linearly with the decrease of  $q$

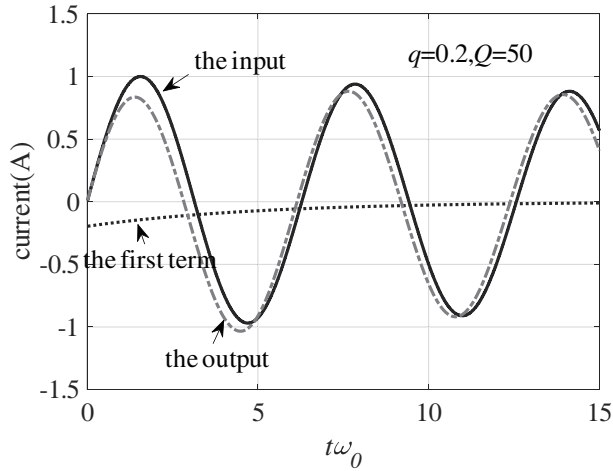


**FIGURE 12.** Output of the model ( $p = +\infty$ ,  $q = 0.2$ ,  $Q = 50$  as an example). Input (solid line) and the newly-emerged exponential decay term (dotted line) are also plotted as a reference.

all the time. Because for certain combinations of  $q$  and  $Q$ , the first peak is smaller than the second peak and is not the peak of the whole waveform any more. Output of the model when  $p \rightarrow +\infty$ ,  $q = 0.2$ ,  $Q = 50$  as an example is shown in Fig. 12. Only the first few cycles are shown in the figure. The time-axis is the product of time and angular frequency. The value of the second peak is larger than the first one for this special case.

### 3.3. Summary and Discussion

In summary, when  $p > 5$ , the relative error of the peak value is less than 2% for  $Q > 2$ . Meanwhile, relative error of the peak value is proportional to  $q$  (i.e.,  $e_p \approx -q$ ) roughly when  $q < 0.1$ .

When a pulse current sensor is applied to measure a signal in the form of damped sinusoid, the  $-3$  dB high frequency  $f_{\max}$  of the measurement system should be larger than 5 times of the fundamental resonance frequency  $f_0$ , while the  $-3$  dB low frequency point  $f_{\min}$  is recommended to be less than 0.02 of  $f_0$ , as shown in (17) and (18).

$$f_{\max} > 5f_0 \quad (17)$$

$$f_{\min} < 0.02f_0 \quad (18)$$

Furthermore, as discussed in Subsection 2.3, for  $q = 0.02$ ,  $p = 5$ , when  $\omega = \omega_0$ , the absolute value of  $H(\omega)$  equals 0.98. Thus, if the constant used to recover the measured signal is calibrated by a sine wave with  $\omega = \omega_0$ , the relative error of the peak value could be smaller.

## 4. MONTE-CARLO SIMULATION

Monte-Carlo method is applied to verify the inherent relationship between  $e_p$  and the bandwidth of the wideband proportional current sensor.

Parameters of  $p$ ,  $q$ , and  $Q$  are uniformly distributed. The value ranges of  $p$  and  $q$  are from 5 to 25 and 0 to 0.02, respectively. With some margin, factor  $Q$  is set as uniformly dis-

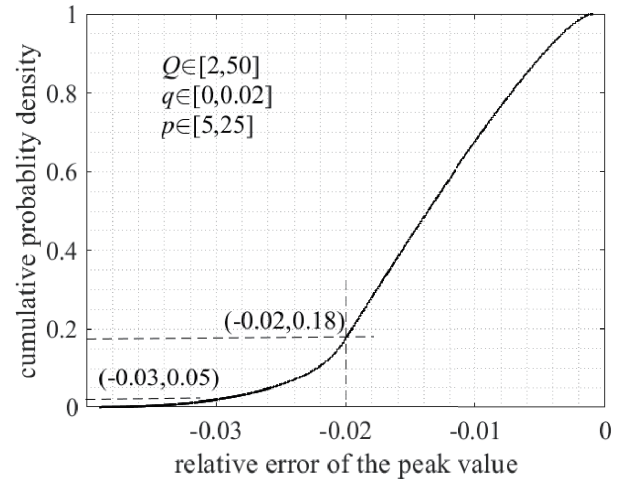


**FIGURE 13.** Cumulative probability density of the relative error of the peak value. The parameters of Monte-Carlo simulation are tagged in the Figure.

tributed from 2 to 50. The number of repetitions is  $10^6$ . The proportional wideband sensor is modeled as the cascade of a low-pass filter and a high-pass filter as shown in Fig. 4. The statistical result is shown in Fig. 13.

The result shows that when  $p > 5$  and  $q < 0.02$  simultaneously, the probability of  $e_p < 2\%$  is 92%, and the probability of  $e_p < 3\%$  is 95%. The error is negligible for engineering practice. Thus, the recommended bandwidth requirements ((17) and (18)) are reasonable for damped sinusoid pulse measurement.

Two examples are provided to illustrate how the formulae applied to measure the injected and coupling damped sinusoid current. For example, according to MIL STD-461F [4], CS116 immunity test should be conducted at six frequencies, i.e., 10 kHz, 100 kHz, 1 MHz, 10 MHz, 30 MHz, and 100 MHz. To measure these injected damped sinusoids by a proportional current sensor, the  $-3$  dB bandwidth of the sensors should cover 200 Hz  $\sim$  50 kHz, 2 kHz  $\sim$  500 kHz, 20 kHz  $\sim$  5 MHz, 200 kHz  $\sim$  50 MHz, and 2 MHz  $\sim$  500 MHz, respectively. As another example, assuming that there is a monopole antenna above infinite metal plate, the length of the monopole antenna is 5 m ( $f_0$  is 15 MHz approximately), then the  $-3$  dB bandwidth needed to measure the coupling current of the antenna should cover 300 kHz  $\sim$  75 MHz.

Furthermore, the parameters of the exponentially damped sinusoids can be estimated by the methods proposed in [10, 11] once the signal is measured. The formulae proposed in this paper are useful for the testers on site to double check the measurement results during HEMP immunity test.

## 5. CONCLUSION

Proportional current sensors are commonly-used in HEMP conducted immunity test for their simplicity and convenience. Based on HEMP practical application, two simple formulae ((17) and (18)) are provided to estimate the bandwidth requirements of the measurement system for damped sinusoid mea-

surement. When a pulse current sensor is applied to measure a signal in the form of damped sinusoid, the  $-3$  dB high frequency  $f_{\max}$  of the measurement system should be larger than 5 times of the fundamental resonance frequency  $f_0$ , while the  $-3$  dB low frequency point  $f_{\min}$  is recommended to be less than 0.02 of  $f_0$ .

The conclusion can be applied as the guideline of pulse current sensor selection for damped sinusoid measurement. The conclusion is useful for the testers on site to double check the measurement system during HEMP immunity test.

## APPENDIX A.

The output of the current sensor in frequency domain can be expressed as (A1).

$$I_{out}(\omega) = kI_p \frac{j\omega}{j\omega + \omega_{lo}} \frac{\omega_{hi}}{j\omega + \omega_{hi}} \frac{\omega_0}{(\omega_0/2Q + j\omega)^2 + \omega_0^2} \quad (\text{A1})$$

(A1) can also be written as (A2).

$$I_{out}(\omega) = kI_p \left[ \begin{array}{c} \frac{A}{j\omega + \omega_{lo}} + \frac{B}{j\omega + \omega_{hi}} \\ + \frac{C(j\omega + \omega_0/2Q)}{(\omega_0/2Q + j\omega)^2 + \omega_0^2} \\ + \frac{D\omega_0}{(\omega_0/2Q + j\omega)^2 + \omega_0^2} \end{array} \right] \quad (\text{A2})$$

Then, the method of undetermined coefficients (MUC) is applied to obtain the coefficients. Inverse Fourier transformation is applied to obtain the output of the current sensor in time domain.

$$I_{out}(t) = kI_p \left[ \begin{array}{c} A \exp(-\omega_{lo}t) u(t) \\ + B \exp(-\omega_{hi}t) u(t) \\ + C \exp(-\omega_0 t/2Q) \cos(\omega_0 t) u(t) \\ + D \exp(-\omega_0 t/2Q) \sin(\omega_0 t) u(t) \end{array} \right] \quad (\text{A3})$$

Furthermore, through trigonometric function operation, (A3) can be expressed as (13).

## REFERENCES

- [1] IEC 61000-2-9, "Electromagnetic compatibility (EMC) - Part 2-9: Environment Description of HEMP environment-radiated disturbance," 1996.
- [2] IEC 61000-2-10, "Electromagnetic compatibility (EMC) - Part 2-10: Environment Description of HEMP environment-conducted disturbance," 1999.
- [3] IEC 61000-4-25 Ed. 1.0, "Electromagnetic Compatibility (EMC) - Part 4: Testing and measurement technique-Section 25: HEMP immunity test methods for equipment and system," 2012.
- [4] Department of Defence, MIL-STD 461F, "Requirements for the control of electromagnetic interference characteristics of subsystem and equipment," 2007.
- [5] IEC 61000-4-18 Ed. 2.0, "Electromagnetic Compatibility (EMC) - Part 4: Testing and measurement technique-Section 18: Dampes oscillatory wave immunity test," 2019.
- [6] Yang, J., Z. Cui, F. Cao, Z. Zhu, C. He, and M. Qiu, "Estimation method of bandwidth requirements for double exponential pulse measurement," *IEEE Transactions on Electromagnetic Compatibility*, Vol. 65, No. 6, 1981–1989, Dec. 2023.
- [7] Yang, J., Z. Z. Zhu, Y. W. Shi, Z. T. Cui, W. Wu, and W. Chen, "Engineering estimation of the upper and the lower limits of  $-3$  dB pass band frequency of wideband measurement system," *Modern Applied Physics*, Vol. 13, No. 2, 020 201–1–8, Jun. 2022.
- [8] Pearson Electronics, Inc, "Pearson™ Current Monitor Model 8585C," Available: <http://pearsonsensor.com/zil/8585C.pdf>.
- [9] McClellan, J. H., R. W. Schafer, and M. A. Yoder, *Signal Processing First*, Prentice Hall, 2003.
- [10] Xu, H., S. Zhou, and B. Yan, "Parameter estimation for a damped real-valued sinusoid in noise," *Review of Scientific Instruments*, Vol. 92, No. 8, 085103, 2021.
- [11] Agrez, D., "A frequency domain procedure for estimation of the exponentially damped sinusoids," in *2009 IEEE Instrumentation and Measurement Technology Conference*, 1321–1326, Singapore, 2009.